**Versão do arquivo anexado / Version of attached file:**

Versão do Editor / Published Version

**Mais informações no site da editora / Further information on publisher's website:**

https://www.sciencedirect.com/journal/carbon-trends/vol/9/suppl/C

**DOI: 10.1016/j.cartre.2022.100226**

**Direitos autorais / Publisher's copyright statement:**

# From radicals destabilization to stable fullerenol nanoaggregates ☆

João Paulo V. Damasceno*, Lauro T. Kubota*

*Department of Analytical Chemistry, Laboratory of Electrochemistry, Electroanalytics and Sensor Development (LEEDS), Institute of Chemistry (IQ), State University of Campinas 13084-971, Brazil*

A B S T R A C T

Fullerenols are fullerenes derivatives enriched on hydroxyl groups that are obtained usually as nanoaggregates dispersed in water. These materials are used in energy-related and biological applications, and they have been reported as radical scavengers, antioxidants and stable radicals. However, most syntheses demand highly toxic solvents to dissolve precursor fullerene, potentially dangerous reagents such as hydrogen peroxide, and prolonged reactions. Herein, a novel and faster procedure for fullerenol preparation based on the reaction between fullerene $C_{60}$ and potassium hydroxide in a polar solvent is reported. Initially, fullerenol radicals are formed, followed by air oxidation that promotes charge loss and simultaneous clustering into nanoaggregates with diameters up to 90 nm. Dried fullerenol has about 12 oxygenated groups per $C_{60}$. Then, an aqueous dispersion was prepared with dispersed material having lyophobic behavior but maintaining the modification degree. This low-modified fullerenol remains dispersed indefinitely in organic medium due to electrostatic and solvation colloidal interactions arising from the functional groups. As a result, stable organic dispersions with concentrations up to 10 mg mL$^{-1}$ were obtained. This work opens new possibilities on fullerenol preparation and new perspectives concerning the achievement of stable colloids of carbon nanomaterials due to the unprecedented stability and mass concentration of the reported fullerenol dispersions.

## 1. Introduction

Fullerenols are fullerenes derivatives modified with hydroxyl [1–8] and some other minor functional groups like hemiketal, epoxide and carbonyl [3–5]. While fullerenes are soluble in organic and non-polar solvents such as benzene, toluene, $CS_2$, 1-naphthalene, among others [9], fullerenols interact strongly with water and polar organic solvents due to the functional groups [1,3,7]. Surface functionalization provides unique properties to fullerenols as high catalytic activity in electrochemical hydrogen evolution [8] and radical-scavenging ability [10,11]. They have been used as antioxidants [12], stabilizing agents for metallic nanoparticles [13], in drug delivery [14], or to facilitate electron transport in perovskite solar cells [15].

The achievement of stable and concentrated dispersions or solutions of carbon materials without using passivating agents and maintaining their metallic or semiconductor behavior simultane-

ously is still a great challenge. Functionalization efficiently improves the hydrophilicity of carbon-based materials (or lyophilic character), and strong intermolecular interactions with polar solvents allow the preparation of concentrated systems [16,17]. Kokubo et al. [1,2] have prepared highly functionalized fullerenols with approximated formulas $C_{60}(OH)_{36}$, $C_{60}(OH)_{40}$ and $C_{60}(OH)_{44}$, which are soluble in water as individual molecules in concentrations up to 64 mg mL$^{-1}$ under neutral conditions [1,2] due to the high hydrophilicity of these materials. However, surface modification disrupts the electronic structure, resulting in insulator carbon-based materials like graphene oxide [18,19]. Although pristine $C_{60}$ has low electrical conductivity [20], it is semiconductor and this property is fundamental for the applications related to electric, electronic and electrochemical devices. Therefore, surface modifications should be minimized if those applications are intended.

Most works concerning fullerenol preparation report less functionalized materials with up to 26 hydroxyl groups per fullerene unit [1–5,7,17,21]. Such modification degree usually is not enough to provide solubility as individual molecules and much less concentrated systems than those reported by Kokubo et al. [1,2] are obtained, but it contributes to increase the affinity for polar solvents. Low-modified fullerenols are composed by dispersed

nanoaggregates with mean diameters between about 50 and 300 nm [3,5,17,21], mass concentration [3,6,22,23] ranging from 0.075 to 3.5 mg mL$^{-1}$ (or close values usually), and have colloidal properties dependent on the functionalization degree and dispersant [17].

Carbon-based colloids without passivating agents as these fullerenol nanoaggregates are stabilized mainly by solvation and electrostatic interactions [16], and both are linked with the presence and concentration of functional groups. While solvation is generated by intermolecular interactions between modified surface and solvent molecules, electrostatic stabilization is achieved when charged functional groups are bonded to the surface such as deprotonated hydroxyl groups reported for fullerenol nanoaggregates in water [5,7,8,23]. The advantage of this stabilization is the preparation of stable carbon-based dispersions (or metastable for long periods) without modifying the surface significantly. Since small amounts of charges (or charged groups) are enough for colloidal stability [24,25], the low modification of such systems preserves part of the electronic structure and conductivity.

Stable fullerenol dispersions composed of low functionalized nanoaggregates have been reported by different authors. Most preparation routes are based on monophasic systems using pristine fullerene $C_{60}$ [3] or low modified fullerenol [1] and hydrogen peroxide in water, or biphasic ones using toluene to dissolve fullerene $C_{60}$, plus sodium hydroxide [5,26] or hydrogen peroxide [27], and tetrabutylammonium hydroxide as phase catalyst. However, these procedures are based on prolonged treatments [1,5,6,27], highly toxic solvents as toluene [5,27], and/or potentially dangerous reagents as hydrogen peroxide [1,2,27]. Therefore, novel preparation routes have to be proposed to bring fullerenol syntheses closer to the principles of Green Chemistry.

In this work, we have reported the achievement of a stable fullerenol dispersion using pristine $C_{60}$, potassium hydroxide and N,N'-dimethylformamide (DMF) under inert atmosphere and at ambient temperature. In the first step, this mixture produces fullerenol radicals unstable towards oxygen. After oxidation by air, the destabilization of these radicals induces aggregation into nanostructures, and oxidation also increases the functionalization degree of the fullerenols. The modification degree of the final material has been probed as about 12 oxygenated functional groups per $C_{60}$ cage. Those oxygenated groups provide colloidal stability for fullerenol nanoaggregates, which are stabilized by solvation and electrostatic interactions and present lyophilic behavior in DMF. Such high affinity for the solvent has allowed the preparation of fullerenol colloids with concentrations up to 10 mg mL$^{-1}$. Next, an aqueous fullerenol dispersion was prepared using the organic solution of fullerenol radicals. After water transfer, the dispersed material presents lyophobic behavior but maintains a low functionalization degree. Finally, we have proposed a simplified mechanism for fullerenol synthesis and nanoaggregate formation based on the experimental evidences.

## 2. Experimental section

### 2.1. Materials

Fullerene $C_{60}$ (99.5 %), N,N'-dimethylformamide (DMF) (99.8 %, anhydrous), potassium hydroxide ($\geq$ 90 %, flake), tetrabutylammonium hydroxide (TBAH) ($\geq$ 99.0 %) were acquired from Sigma-Aldrich, and potassium chloride (99.0 %) from Vetec. All aqueous solutions and dispersions were prepared with deionized water collected in a Millipore equipment, model Direct-Q 3UV, with electrical resistivity higher than 18.2 M$\Omega$ cm. Stirring plates from Heidolph, model MR Hei-Tec, with a maximum stirring speed of 1400 rpm and heating capacity up to 300 °C were used to prepare fullerenol and KOH mixtures.

### 2.2. Modification of $C_{60}$ with KOH in DMF and preparation of organic dispersion

Fullerene $C_{60}$ modification with KOH was conducted based on the literature [28]. Briefly, 78 mg of KOH and 20 mL of DMF were added in a 50 mL round-bottom glass flask. This mixture was stirred at 500 rpm under $N_2$ purge for 5 min (keeping a polymeric cannula inside DMF solution). After that time, 20 mg of fullerene $C_{60}$ was added to the mixture, and the stirring and purge were kept for 1 h (ambient temperature). At the end of this period, a dark purple mixture was obtained with remaining solid $C_{60}$ and KOH at the bottom of the flask. The supernatant (sample A) was added to another glass flask without solid material. After exposition to atmospheric air, the purple mixture turns gradually into dark brown, indicating the formation of fullerenols. It was stored in a glass vial and named as sample B.

### 2.3. Preparation of aqueous fullerenol dispersion

The aqueous dispersion was prepared using a similar procedure from the literature to prepare aqueous fullerene dispersions [17]. Deionized water (18 mL) was added to a glass vial and sample A fresh oxidized (just after air exposition) was added slowly in two portions of 1 mL each, resulting in aqueous fullerenol dispersion (10 % in volume). A colour change from purple to brown was observed after transferring the DMF mixture to water, indicating the formation of fullerenol dispersion. It was stored in a glass vial and named as sample C.

### 2.4. Solid fullerenol samples

Sample B was transferred to a clean watch glass and dried at 50 °C using a hot plate inside a fume hood, avoiding dust and other impurities. The recovered solid was named sample D. Most of the sample characterization was conducted with this fullerenol dried at 50 °C (sample D), except Fourier-transform infrared spectroscopy (FTIR) that was performed with a sample prepared as described before and dried at 150 °C in an oven (after drying at 50 °C) to remove most of DMF. A similar drying procedure was applied to aqueous fullerenol (sample C), prepared following the previous procedure but with only 20 % of water (volume) instead of 90 % in the conventional procedure. This sample was dried at 50 °C just after water addition, and the recovered solid was named sample E.

### 2.5. Homocoagulation experiments with organic dispersion (sample B) and aqueous dispersion (sample C)

Homocoagulation experiments were conducted using sample B (organic dispersion) mixed with solutions of TBAH in DMF with different concentrations or using sample C (aqueous dispersion) mixed with aqueous solutions of KCl with different concentrations. The mixtures were prepared by adding 900 µL of the respective dispersions and 900 µL of the respective electrolyte solution, which are 2 times more concentrated than the desired final concentration, in 2 mL glass vials. One mixture was prepared using the respective pure solvent (no salt) and the final electrolyte concentrations in both sets of experiments were equal to $5\times10^{-6}$, $1\times10^{-5}$, $5\times10^{-5}$, $1\times10^{-4}$, $5\times10^{-4}$, $1\times10^{-3}$, $5\times10^{-3}$, $1\times10^{-2}$, $5\times10^{-2}$ e $1\times10^{-1}$ mol L$^{-1}$ (already considering the dilution by a factor of 2 due to mixing with equal volumes of dispersion and electrolyte solution). Samples were homogenized by hand and left to rest for 12 h. After that period, pictures were taken to register the homocoagulation results.
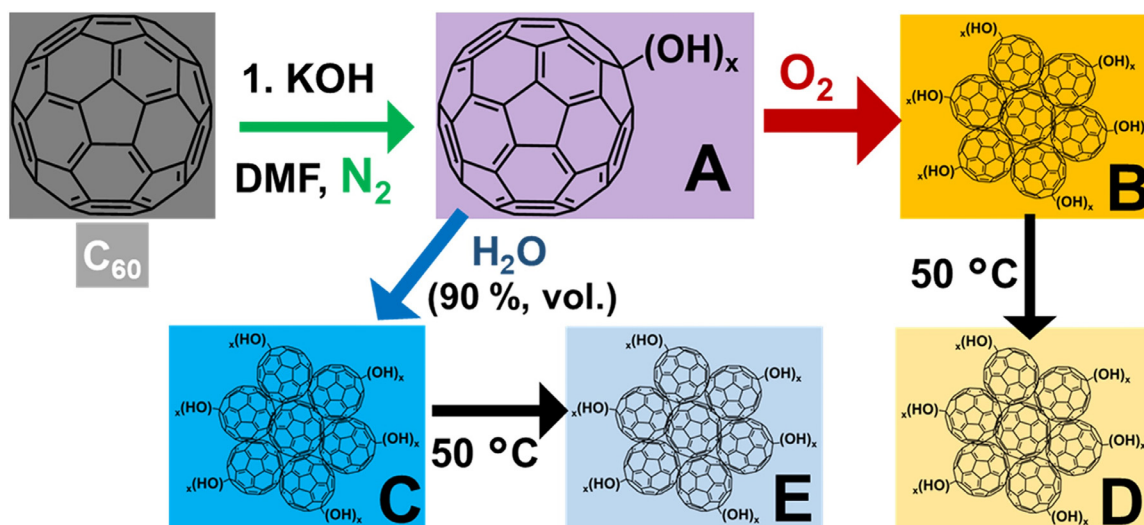
**Fig. 1.** Schematic representation of fullerenol preparation: (i) modification of fullerene $C_{60}$ with KOH in DMF purged with $N_2$ (step 1; sample A), followed by $O_2$ oxidation and formation of nanoaggregates (sample B); water transfer to produce aqueous dispersion (sample C); Drying process of samples B and C to obtain the respective solid fullerenols (samples D and E, respectively).

## 2.6. Concentrated organic dispersion

Freshly oxidized fullerenol (sample A) was transferred to a round-bottom glass flask and DMF was removed using a rotary evaporator with water bath at 50 °C and pressure of 3-5 mbar. After evaporating most of the solvent (about 95 %), a concentrated liquid mixture was obtained with concentration close to 10 mg $mL^{-1}$. Therefore, to collect an appreciated volume of this concentrated dispersion, it is necessary to start with about 200 mL of sample A. In this case, sample A was synthesized using 10 times of each reagent and solvent, and using a 200 mL glass flask. This mixture was stirred and purged for 4 h.

## 3. Results and discussion

A new procedure to obtain stable fullerenol dispersions is reported by combining two experimental evidences from the literature: (i) KOH reacts with $C_{60}$ in DMF and produces fullerenol radicals like $[C_{60}(OH)_x]^-$ [28], and (ii) organic solutions of fullerides ($C_{60}^{n-}$, n = 1 or 6) can be oxidized with $O_2$ and produce stable fullerene dispersions with variable content of fullerenols [17]. Fig. 1 shows a schematic representation of the fullerene modification. The first step of fullerenol preparation was adapted from the literature [28] and conducted by mixing $C_{60}$ and KOH in DMF under inert atmosphere (sample A) (details in the Experimental section). In the second step, the supernatant was transferred to another glass flask, exposed to atmospheric air to promote oxidation and stored at least 1 day before analysis (sample B). Some hours after the contact with atmospheric air, fullerenol nanoaggregates are formed and reach a stable state. The supernatant containing fullerenol was also used to prepare aqueous fullerenol dispersion (sample C) just after air oxidation (details in SI). Both dispersions were dried to obtain solid fullerenols (samples D and E, respectively).

Naim and Shevlin have reported the reversible modification of fullerenes $C_{60}$ and $C_{70}$ with KOH in toluene [29], and Litvinov et al. have used KOH as a modifier for $C_{60}$ in DMF to prepare fullerenol radicals [28]. Contact of fullerene $C_{60}$ with KOH in DMF under $N_2$ atmosphere produces a dark purple supernatant after 1 h, as Fig. S1 presents. After air exposition, this dark purple mixture slowly changes to dark brown, which is the first indication of the fullerenol formation. The reaction between $[C_{60}(OH)]^-$ (formed af-

ter hydroxide addition to fullerene) and pristine $C_{60}$ can occur, and it produces $C_{60}^-$, because the first is a stronger donor according to the literature [28]. However, $C_{60}^-$ is the minor product and the formation of $[C_{60}(OH)_x]^-$ is favored when the reaction is conducted in DMF [28]. These reactions occur due to the lower standard reduction potential of $C_{60}$ in DMF [30,31]. Meanwhile, in other solvents like THF or acetonitrile the mixture of $C_{60}$ and KOH results in light brown suspensions, indicating the formation of diluted dispersions (or suspensions) without molecular intermediates like $[C_{60}(OH)_x]^-$, which are important for increasing mass concentration as well as the functionalization degree.

Fig. 2A presents the UV-Vis-NIR spectrum of sample A. Bands at 993 and 1074 nm are referent to $C_{60}^-$ anion [17,28,30–32], and at 927 and 1034 nm are attributed to fullerenol radicals. Similar absorptions were observed for $[C_{60}(OH)_x]^-$ reported by Litvinov et al. [28] and for $[C_{60}(OH)_{18}]^-$ reported by Mohan et al. [21]. These fullerene and fullerenol radicals are unstable in the presence of oxygen. The intensities of NIR bands decrease gradually due to air exposition until they completely vanish after about 6-8 h, as present in the spectra of Fig. 2B. The spectrum of sample B in Fig. 2A does not present bands in the NIR region, which indicates the absence or very low concentration of radicals.

Sample A exhibits intense absorption bands below 400 nm and weak absorptions between 450 and 650 nm, which are also present in the spectra of $C_{60}$ solution in DMF (Fig. 2A) and in toluene (Fig. S2). These bands are referent to allowed and prohibited electronic transitions, respectively [20,33]. They are also present in the spectrum of fullerene anions ($C_{60}^{n-}$), since the formation of anions does not alter the electronic structure of fullerene in great extent [34]. However, these bands became less defined after oxidation as Fig. 2A shows, indicating changes in the electronic structure caused probably by the surface modification of the carbon material on sample B.

According to the literature [35], the presence of $O_2$ in mixtures of $C_{60}$ and $OH^-$ contributes to increase fullerene hydroxylation because oxygen can capture electrons from $C_{60}^-$ or $[C_{60}(OH)_x]^-$ anions allowing further reactions with hydroxide. The spectra from Fig. 2 corroborate this charge loss by oxygen. Similarly, the contact between $C_{60}^-$ and $O_2$ also results in surface modification with oxygenated groups [17]. The gradual increment in the broad absorption between 400 and 500 nm along time presented in Fig. 2B indicates the formation of dispersed fullerene nanostructures [17,36]
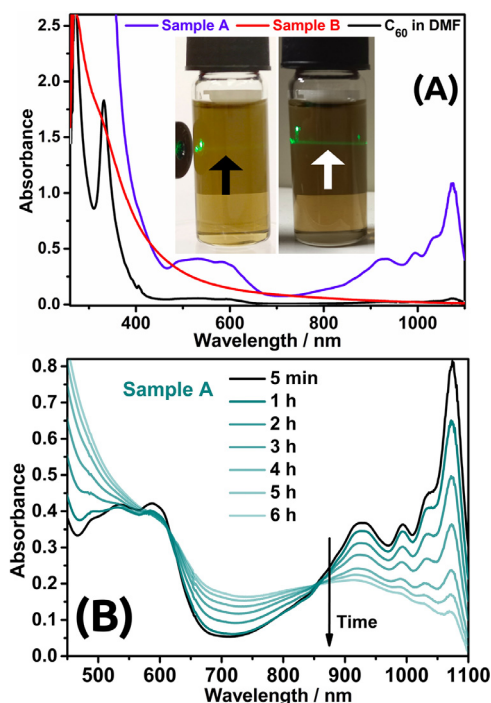
**Fig. 2.** UV-Vis-NIR spectra of sample A (before oxidation) and sample B (after oxidation); inserted: picture of diluted sample B (20 % in DMF) irradiated with green laser and under ambient (left) or reduced illumination (right) (arrow points the laser track) (A). UV-Vis-NIR spectra of sample A obtained in the first 6 h after the synthesis keeping the cuvette partially open to atmosphere (small aperture) (B).



**Fig. 3.** DLS result for sample B in DMF (A); Image of atomic force microscopy (AFM) acquired in topography mode of sample B over a silicon substrate (B).

and/or low hydroxylated fullerenols [1,6,27]. Therefore, the radicals destabilization by oxygen has a fundamental role in increasing the functionalization degree and also in the formation of nanoaggregates.

The picture inserted in Fig. 2A shows that diluted sample B (20 % in DMF; sample B is dark brown, and scattering is visible only in diluted mixtures) presents a weak Tyndall effect (arrow), which indicates the presence of dispersed material. The laser track is very weak under ambient light (left picture), but when the ambient light is reduced the scattering can be seen (right picture). Such weak scattering indicates small particles and/or lyophilic behavior for sample B. Similar scattering is observed for sample C, but much stronger as presented in Fig. S3. Samples B and C have mass concentrations of 0.41 and 0.04 mg mL$^{-1}$ respectively (after subtracting potassium content). Indeglia et al. [37] have conducted a detailed study probing that fullerenols with mildly modification degree (up to 24 oxygenated groups per fullerene cage) exist as individual molecules in neutral aqueous solution at concentrations below 0.002 mg mL$^{-1}$ (2 mg L$^{-1}$), therefore it is expected that the prepared organic and aqueous dispersions are mainly composed by nanoaggregates.

Dynamic light scattering (DLS) result is presented in Fig. 3A in terms of number intensity as a function of size instead of scattering intensity as recommended by Kokubo for DLS analysis of soluble fullerenols [2,35]. DLS measurement confirms that sample B is formed by nanoaggregates. These nanostructures have two size distributions, with lognormal profiles, one between 6 and 10 nm and the other between 60 and 90 nm, with mean sizes of 8.2 nm and 76 nm, respectively. This bimodal distribution was also observed by Indeglia et al. [37] in concentrated fullerenol dispersions.

A solution was prepared by stirring pristine fullerene C$_{60}$ in DMF under nitrogen purge to evaluate the presence of nanoclusters. This mixture presents a light pink color after centrifugation, but it turns into light yellow a few hours after the preparation,
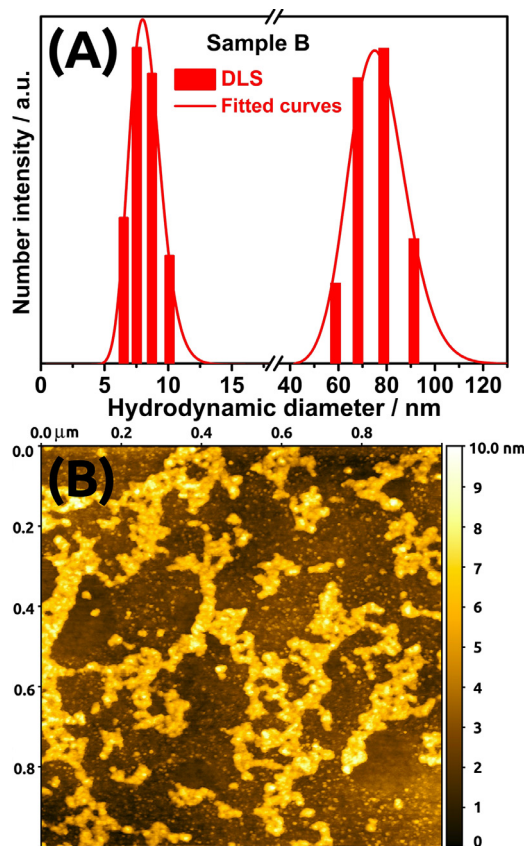
indicating the presence of dispersed C$_{60}$. Nanoclusters with sizes between 85 and 140 nm are present in the freshly centrifuged mixture as Fig. S4 shows, which is expected because C$_{60}$ is not soluble in DMF in a great extent. However, those aggregates can be present just after preparation (in the pink mixture) or can be produced after oxygen exposition during the DLS analysis. DLS result for sample A has a similar tendency as Fig. S4 shows, with sizes between 25 and 50 nm. However, the presence of nanoaggregates at the beginning of the reaction between C$_{60}$ and KOH cannot be disregarded, as well as the presence of nanostructures in sample A just after the contact with oxygen.

Since no passivating agent was added to control particle morphology, spherical particles were expected in sample B. The SEM image from Fig. S5 corroborates the formation of fullerenol nanoaggregates with spherical-like morphology after oxidation. Individualized particles shown in the SEM image present sizes of the same order of magnitude as those values determined by DLS. Still, they are usually larger due to the aggregation that occurs during the sample drying. Some aggregates are larger and have micrometric sizes also due to the drying process.

AFM image presented in Fig. 3B confirms the spherical morphology of fullerenol nanoclusters from sample B, which has aggregates with mean height next to 8 nm corroborating the DLS results. Image from Fig. 3B also presents small particles seen as dots with heights of about 1.2 to 1.4 nm, and they are attributed to individual fullerenol molecules, which is in accordance with the value of 1.34 nm reported by Indeglia et al. [37] The presence of individual fullerenol molecules is due to the favorable intermolecular interactions between the functional groups from fullerenol surface and the solvent molecules. Pristine C$_{60}$ does not interact to
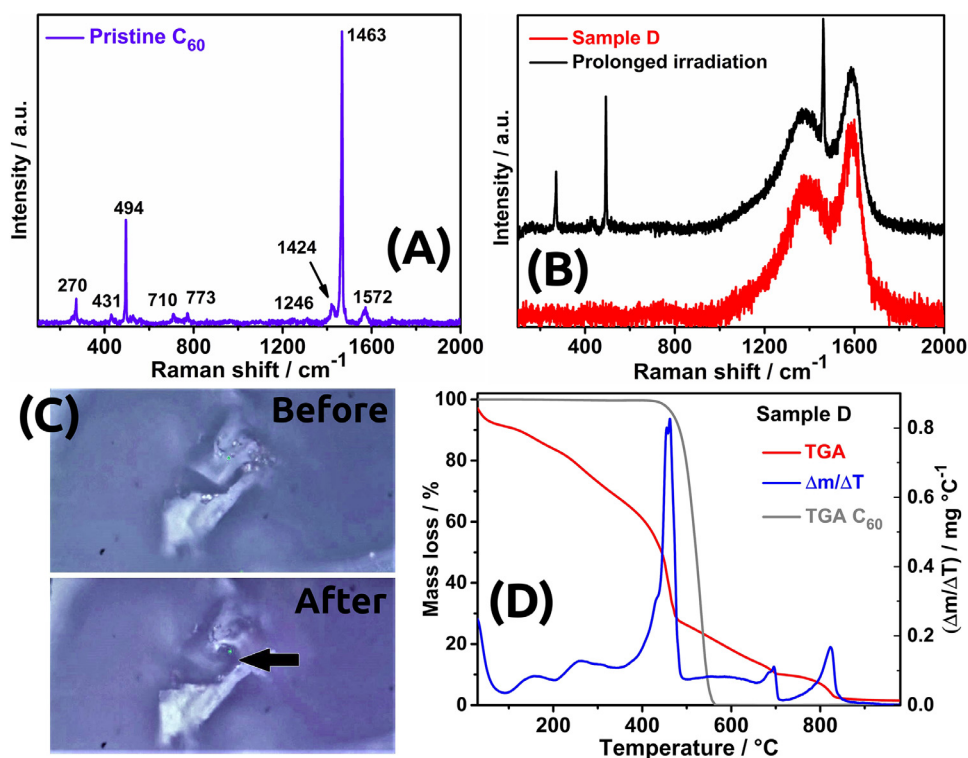
**Fig. 4.** Raman spectrum of pristine $C_{60}$ (A); Raman spectra of sample D acquired with low power or using high power and prolonged irradiation (B); Optical images of sample D before and after Raman analysis using prolonged irradiation (C); Curves of mass loss as a function of temperature for sample D dried at 50 °C and pristine $C_{60}$ (D).

a great extent with DMF and tends to produce larger particles in such medium as DLS result has shown. The coexistence of individual molecules and nanoaggregates presented in the AFM image from Fig. 3B and the mean diameter as a function of mass concentration reported in the literature [37] suggest that fullerenol molecules are not irreversible bonded to each other, which indicates that hydrophobic or similar non-covalent interactions are responsible for the cohesion of fullerenol molecules in each cluster.

Raman spectrum of pristine $C_{60}$ is presented in Fig. 4A and shows the characteristic Raman modes at room temperature [38]. Sample D was prepared by drying sample B. It has much less intense Raman modes, as shown in Fig. 4B, with a profile similar to carbon materials with high defect concentration like graphene oxide [39] or pyrolytic carbon materials [40]. This Raman profile is in accordance with that reported by Santiago et al. [27] and by Ravelo-Nieto et al. [41] and it corroborates the formation of fullerenols. The insertion of functional groups on $C_{60}$ surface decreases the molecule symmetry. Therefore, novel modes are expected to appear and most probably with lower intensity [20,42]. Different points of sample D presented the same spectral profile when Raman spectrum was acquired using low laser power, with a low number of accumulations and less exposition time (*e.g.* 2 ac. of 10 s each using 0.16 mW). Therefore, the spectrum from Fig. 4B can be assigned as the Raman profile of fullerenol (sample D).

When a single spot was irradiated by prolonged time and using higher power (*e.g.* 5 ac. of 30 s each using 0.65 mW), narrow bands were produced and they coexist with the broad ones as Fig. 4B presents. These narrow signals have maxima at 270, 493 and 1462 $cm^{-1}$ and are attributed to the fullerene Raman modes, which indicates that $C_{60}$ was partially regenerated probably due to the loss of functional groups during laser irradiation. The $A_g$ mode at 1462 $cm^{-1}$ is the pentagonal 'pinch' and is characteristic of the icosahedral structure, whereas the $A_g$ mode at 493 $cm^{-1}$ is the breathing mode and confirms the maintenance of the cage-like structure [20]. Raman spectra of fullerene derivatives can be found in the

early literature, and since that time the decomposition of samples during analysis was not ruled out [42]. Changes in sample D can be visualized by optical images presented in Fig. 4C, which were acquired before and after the Raman analysis. The dark spot was formed after prolonged laser irradiation and corroborates sample changes.

Raman profile from Fig. 4B could be attributed to graphitic structures since the fullerene cage could open after the modification with functional groups. However, the emergence of those narrow bands after prolonged irradiation indicates that the icosahedral structure is maintained after modification with KOH. Otherwise, these bands would not be formed, and a graphitic-like profile would be observed. The maintenance of the cage structure after surface functionalization is in accordance with AFM image from Fig. 3B, which presents spherical particles. The height of individual objects with spherical morphology are characteristic of fullerenol. Graphene oxide or fullerene fragments, which can be compared to molecules such as corannulene [43], should have lower height. Therefore, the spectral changes observed for sample D are attributed to the lower symmetry of fullerenol compared to pristine $C_{60}$.

FTIR spectrum of pristine $C_{60}$ is presented in Fig. S6 and it shows four vibration modes with maxima at 527, 576, 1183 and 1429 $cm^{-1}$, which is in accordance with the literature [44]. The spectrum of sample D presented in Fig. S7 has a different profile with bands at 1098 and 1384 $cm^{-1}$ referent to $\nu$C-O and $\delta_S$C-O-H vibrations. A narrow band with intensity maximum at 1652 $cm^{-1}$ is attributed to $\nu$C=C mode. A large band at 3450 $cm^{-1}$ with a shoulder at 3250 $cm^{-1}$ is assigned to O-H vibrations [2,4,6,11,23,27,45] due to ambient water and hydroxyl groups from fullerenol. Differently from other reports [2,11], there is no signal at about 1700 $cm^{-1}$ (sample without DMF, dried at 150°C), which indicates a low content of carbonyl or carboxyl groups attached to the fullerenol surface. Nevertheless, both Raman and FTIR results corroborate fullerene modification.
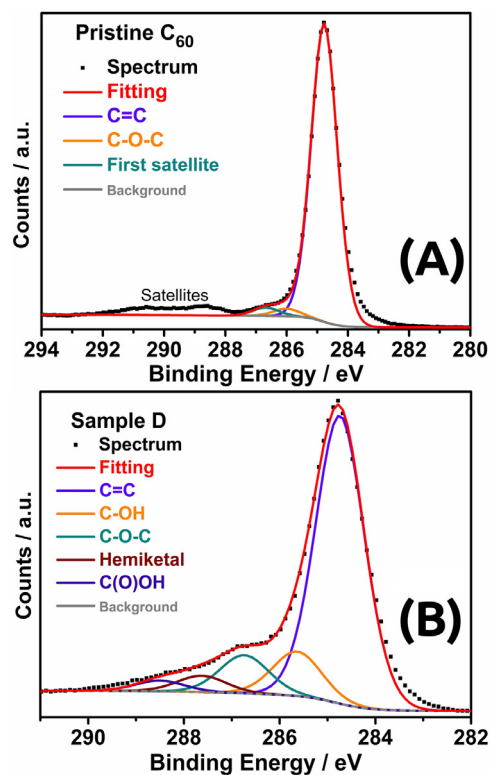
**Fig. 5.** Carbon 1s XPS spectra of pristine fullerene $C_{60}$ (A) and sample D (B).

Thermogravimetric analysis (TGA) of pristine $C_{60}$ exhibits a single mass loss between 430 and 560 °C as presented in Fig. 4D, which corresponds to the carbon combustion [46,47]. In contrast, TGA for sample D presented in Fig. 4D has eight processes of mass loss, and this profile confirms fullerene modification (details in SI) [1–4,6,27]. Thermogravimetric analyses (TGA) of samples D and E are presented in Fig. S8, and they show that there is almost no difference between both samples since the distinct profile up to 200 °C is attributed to remaining DMF in sample D. TGA and elemental analysis (CHN) of these two samples (details in SI) revealed that both dried samples (D and E) have similar composition. It means that water in contact with the supernatant enriched in fullerenols (sample A, freshly oxidized) does not increase the modification degree.

X-ray photoelectron spectroscopy (XPS) revealed the concentration and types of functional groups formed on fullerenol. Carbon 1s XPS spectra of pristine fullerene and sample D are presented in Fig. 5A and 5B, respectively. Fullerene $C_{60}$ has one strong signal (97.8 %) referent to $sp^2$ carbon (284.8 eV) and the characteristic shakeup satellites [48] starting at approximately 286.7 eV (difference of 1.9 eV between the first satellite and the main peak) [20]. There is a small contribution (2.2 %) of oxygenated carbon (286.0 eV) that can be attributed to C-O-C groups formed by the reaction with oxygen, since $C_{60}$ was stored under ambient atmosphere. Shulga et al. [49] have reported the oxidation of fullerene by interstitial oxygen and the formation of oxidized species with generic formula $(O_2)_xC_{60}$, which are probably responsible for that XPS signal. Sample D presents more signals referent to oxygenated carbon and lower content of $sp^2$ carbon (72.2 %) due to the surface modification. Other four carbon peaks are present in the XPS spectrum of sample D besides the peak at 284.7 eV, and they are attributed to (i) monohydroxylated carbon (C-OH; 285.7 eV) (11.9 %), (ii) monooxygenated carbon (C-O-C; 286.8 eV) (9.1 %), (iii) dioxygenated carbon (hemiketal; 287.6 eV) (4.1 %), and carbon of carboxylic or similar groups (288.5 eV) (2.7 %) [5,26,37,50,51].

TGA, CHN and XPS results indicate stoichiometry close to $K[C_{60}(OH)_{3-5}(O)_{7-9}]DMF$ for sample D, which represents a mean number of 12 functional groups per fullerene (details in SI). DMF content in the solid material can be variable and is lower for solids dried at higher temperatures or stored for prolonged periods. Since fullerenols with such low functionalization degree are poorly soluble in polar organic solvents or water [1], this stoichiometry is attributed to the mean composition of the nanoaggregates from sample B and not as individualized species like $K[C_{60}(OH)_4(O)_8]$. These insoluble fullerenol molecules aggregate into nanoclusters after air exposition. However, the aggregation tends to stop or become very slow due to the formation of a stable colloid, as observed for sample B.

Although the contact with water does not increase the modification degree of fullerenols appreciably, it changes the colloidal properties of the resultant dispersion. The result of homocoagulation experiment conducted using sample C and KCl solutions is presented in Fig. 6A and indicates that the aqueous colloid has lyophobic nature. Therefore, it is mainly stabilized by electrostatic repulsion. An energy barrier against aggregation of about $26 \times k_B T$ was estimated using Derjaguin-Landau-Verwey-Overbeek (DLVO) theory for spherical particles [24] (Fig. S9) (calculation details in SI). Such barrier provides kinetic stability enough for material processability. This dispersion has been stored for 4 months at room temperature, avoiding evaporation and excessive light exposition.

Sample C is formed by nanoaggregates with diameters between 20 and 200 nm as presents the DLS result from Fig. 6B. UV-Vis spectrum of sample C is presented in Fig. S10 and also shows a broad band between 400 and 500 nm that is characteristic of fullerene dispersions and/or low-modified fullerenols. The mean diameter of 90 nm after 7 days of sample preparation increases to 134 and 195 nm after 21 days and 4 months, respectively. Although no visible precipitate was observed, the DLS results presented in Fig. 6B show that the size distribution became wider and the mean diameter has increased after 4 months. After that period, part of the material starts to precipitate slowly. Size increment over time corroborates the lyophilic nature and the kinetical stabilization of sample C instead of thermodynamic stability, since these nanoaggregates are growing over time.

In contrast to the aqueous dispersion, organic fullerenol dispersion (sample B) does not exhibit homocoagulation with organic electrolyte as presented in Fig. 6C. This indicates lyophilic-like nature for fullerenol nanoaggregates in DMF, corroborating the weak light scattering showed in the picture inserted on Fig. 2A, typical of lyophilic colloids. Such types of dispersions are known to be able to produce concentrated systems [16,24,25].

The literature reports variable values for mass concentration of fullerenol dispersions that depends on the solvent and functionalization degree, for example, 0.075 mg mL$^{-1}$ for $C_{60}(OH)_{18-20}$ in water [6], 0.33 mg mL$^{-1}$ for $C_{60}(OH)_8 \cdot 2H_2O$ in DMSO [3], 1.0 mg mL$^{-1}$ for $C_{60}(OH)_{24-28}$ in water [22], up to 3.5 mg mL$^{-1}$ for $Na_2[C_{60}(OH)_{12}(O)_2]$ in water [23]. Based on the lyophilic nature of sample B, it was concentrated in a rotary evaporator (details in SI), and mass concentrations up to 10 mg mL$^{-1}$ were obtained without visible aggregation or precipitation, which is about 24 times more concentrated than the original dispersion and is one of the most concentrated fullerenol dispersion reported in the literature. Considering that lyophobic dispersions produce only diluted systems [16], and the relatively low functionalization degree of sample B compared to other modified carbon materials like graphene oxide, the achievement of such concentrated dispersions is promising in the field of carbon-based inks, and these systems can be used in inkjet depositions or related applications.

Lyophilic-like nature of sample B suggests that the colloidal stability is provided by favorable solvation interactions between the modified surface of the dispersed particles and solvent molecules.
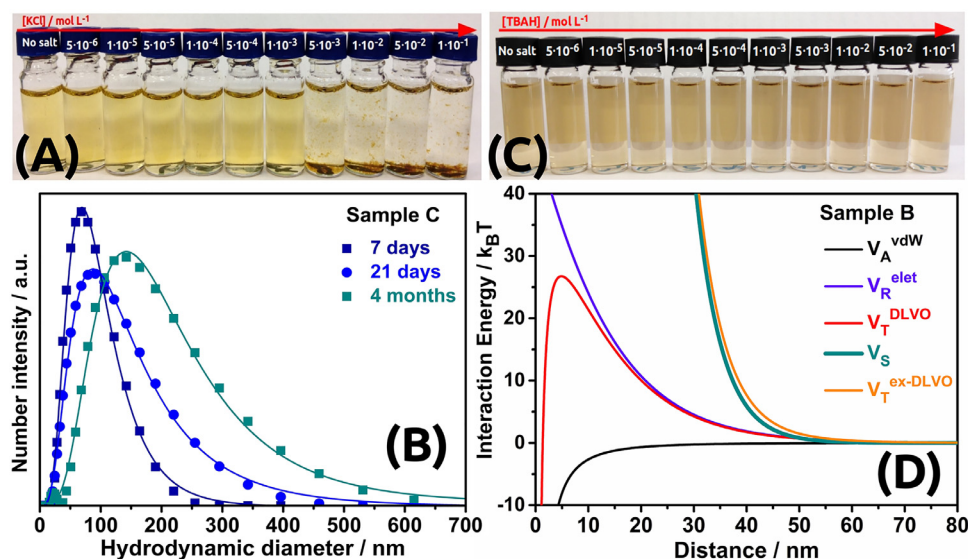
**Fig. 6.** Picture of homocoagulation experiment conducted with sample C mixed with aqueous solutions of KCl in different concentrations as indicated (A); Curves of number intensity as a function of size obtained by DLS measurements of sample C (B); Pictures of homocoagulation experiment conducted with sample B and solutions of TBAH in DMF with different concentrations as indicated (C); Curves of interaction energy as a function of the distance between two particles calculated using DLVO and extended DLVO models for spheres and the experimental values of mean radius and zeta potential of sample B (D).

Besides that, nanoaggregates of this organic dispersion have a mean zeta potential ($\zeta$) of -60 mV, which indicates that they are also stabilized by electrostatic repulsion between electrical double layers. Calculations based on DLVO theory for spherical particles were performed, and the results are presented in Fig. 6D for the original version of the theory and for an extended version that includes the solvation interaction (calculation details in SI). Considering only electrostatic repulsion ($U_R$, positive) and van der Waals (vdW) attraction ($U_A$, negative), the calculation provides an energy barrier next to $27 \times k_B T$ for the total energy of interaction ($U_T$ (DLVO)), close to the value obtained for the aqueous dispersion. However, by including the solvation interaction ($U_S$) (repulsive for this system), Fig. 6D shows a very high repulsion barrier without a maximum value ($U_T$ (ex-DLVO)), which indicates undetermined stability typical of lyophilic systems. The combination of both repulsive interactions, especially solvation opposing the van der Waals attraction, provides indefinite stability for this organic colloid if properly stored (avoiding light, heat, and solvent loss).

Based on the reports by Kokubo [35] and Husebo et al. [5] as well as the experimental results concerning the surface modification and simultaneous formation of nanoaggregates presented in this work, some chemical reactions and a representation of the nanocluster formation are proposed in Fig. 7, which shows a simplified mechanism for the fullerenol preparation. In the first step, hydroxide reacts with pristine $C_{60}$ and produces $[C_{60}(OH)]^-$ (Eq. (1)) under inert conditions. Next, this fullerenol radical can react with available $C_{60}$ (excess) and produce $[C_{60}(OH)]^\bullet$, which is a neutral radical, plus $C_{60}^-$ (Eq. (2)) as indicated by UV-Vis-NIR spectra from Fig. 2. Finally, after air exposure, oxygen reacts with $[C_{60}(OH)]^\bullet$ and $[C_{60}(OH)]^-$ (Eqs. (3) and (4)) resulting in neutral fullerenols like $[C_{60}(OH)]$.

Neutral fullerenol $[C_{60}(OH)]$ can react with another hydroxide and produce more hydroxylated molecules as $[C_{60}(OH)_2]^-$ (Eq. (5)), which reacts with oxygen and starts the cycle again (Eqs. (1)–(4)) until it reaches a mean functionalization degree of about 12 groups per $C_{60}$. In principle, neutral radicals like $[C_{60}(OH)]^\bullet$ also react with hydroxide although not represented in Fig. 7. The reasons why the modification seems to stop are under investi-

gation (total time, temperature), but are not related to limiting reagents because part of $C_{60}$ and KOH remain unreacted at the end of the process (solids mixed with dark purple supernatant (sample A)).

The modification degree is increased only in the presence of oxygen, as indicated by the change in the spectral profile between 190 and 650 nm shown in Fig. 2, since oxygen captures electrons from radicals and allows further hydroxylation [35]. Moreover, other functional groups are generated as the reaction proceeds in the presence of oxygen, which increases the oxidation of some carbon atoms and produces hemiketal or epoxide groups.

When fullerene anion $C_{60}^-$ is exposed to oxygen, it produces $C_{60}$ plus $O_2^-$ (Eq. (6)) [17], and superoxide formed can also react with $C_{60}$ and form $[C_{60}O_2]^-$, similar to the modification of $C_{60}$ with $H_2O_2$ in alkaline medium [35]. $[C_{60}O_2]^-$ can be protonated by ambient water (since atmospheric air was used to oxidize sample A) and reduced to form $C_{60}(OH)$ plus water, similar to the mechanism proposed for the hydroxylation of carbon nanotubides [52], or it can suffer rearrangements and produce two bonded -OH or one -OH plus an epoxide on $C_{60}$ surface.

Oxygen contributes to the radicals destabilization and the resultant neutral fullerenols are insoluble in DMF due to the low modification degree, which induces aggregation into nanoclusters (NCs) (Eq. (7)). About clustering at higher fullerenol concentrations, Indeglia et al. [37] have suggested that the amphiphilic character of fullerenols persists even at high degrees of modification, enabling cluster formation. Since sample A has a higher concentration than the threshold reported by Indeglia et al. [37] and has mean degree of functionalization relatively low, it spontaneously undergoes such clustering after oxygen exposition and nanoaggregates are produced on sample B. The presence of different fullerenol molecules is commonly reported in the literature, and it is under investigation for sample B. However, the probable heterogeneity of the fullerenol prepared in this work is in accordance with the different possible reaction paths and intermediates proposed in Fig. 7 as well as with the formation of nanostructures that protect some fullerenol molecules and expose others to oxygen and hydroxide.

$$C_{60} + OH^- \longrightarrow [C_{60}(OH)]^- \quad (1)$$

$$[C_{60}(OH)]^- + C_{60} \longrightarrow [C_{60}(OH)]^{\cdot} + C_{60}^- \quad (2)$$

$$[C_{60}(OH)]^{\cdot} + O_2 \longrightarrow [C_{60}(OH)] + O_2^- \quad (3)$$

$$[C_{60}(OH)]^- + 2\,O_2 \longrightarrow [C_{60}(OH)] + 2\,O_2^- \quad (4)$$

$$[C_{60}(OH)] + OH^- \longrightarrow [C_{60}(OH)_2]^- \quad (5)$$

$$C_{60}^- + O_2 \longrightarrow C_{60} + O_2^- \longrightarrow [C_{60}(O_2)]^- \quad (6)$$
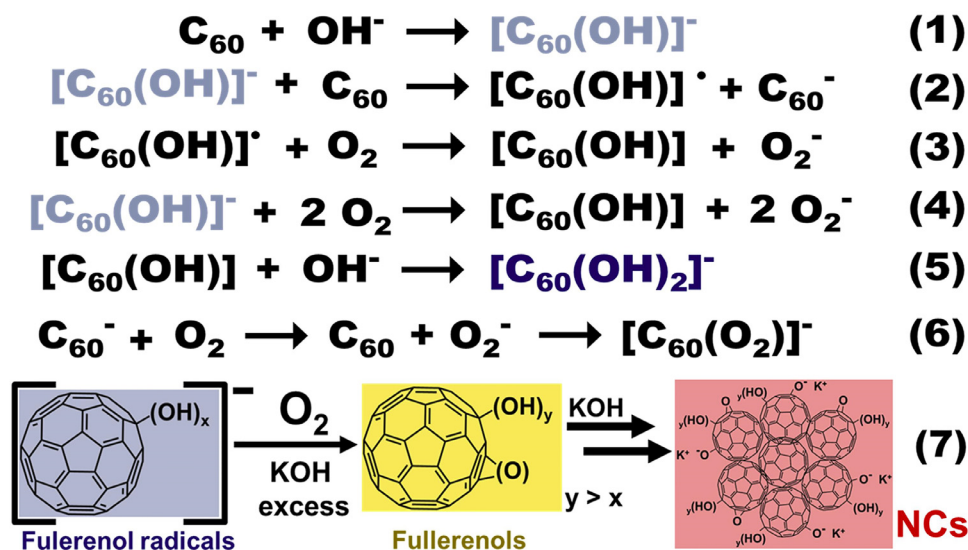


**Fig. 7.** Mechanism of fullerenol formation: possible chemical reactions that can occur during sample preparation under inert (Eqs. (1) and (2)) and oxidizing atmosphere (Eqs. (3)–(6)), and schematic representation of the spontaneous aggregation of low-modified fullerenol molecules into nanoclusters (NCs; Eq. (7)). Charged fullerenol radicals are represented in blue.

Unlike previous reports, our results show that the aggregation tends to stop or become very slow due to the formation of stable fullerenol dispersion that remain dispersed because repulsive colloidal interactions are present. Such interactions emerge only when nanoaggregates are formed. Electrostatic interactions are more relevant for larger particles and small nanoclusters present mainly vdW and solvation interactions. The latter compensates vdW attraction and is the main responsible for stability, especially for very small clusters formed in the beginning of the oxidation. Moreover, both repulsive interactions are related to the presence of functional groups: (i) electrostatic repulsion between double layers of the dispersed particles is generated by deprotonated hydroxyl groups, and (ii) repulsive solvation interaction is due to the high affinity between solvent molecules and fullerenol surface and it provides lyophilic behavior for sample B.

## 4. Conclusion

This work demonstrates a pathway to produce concentrated and stable organic dispersions of fullerenol, which can be prepared in large quantities. Fullerenol was obtained as a stable organic dispersion using a two steps procedure. Initially, fullerenol-based radicals were produced in an organic medium, then air oxidation induced charge loss and the formation of fullerenol nanoaggregates simultaneously. Such dispersion is stable indefinitely because of electrostatic and solvation interactions are present balancing the vdW attraction, and they arise from the functional groups. The colloidal stability of organic fullerenol dispersions (diluted or concentrated) exceed by far the period needed for processability.

## Declaration of Competing Interest

The authors declare that they have no known competing financial interests or personal relationships that could have appeared to influence the work reported in this paper.

## CRediT authorship contribution statement

**João Paulo V. Damasceno:** Conceptualization, Writing – original draft, Investigation, Writing – review & editing. **Lauro T. Kubota:** Investigation, Writing – review & editing.

## Supplementary materials

Supplementary material associated with this article can be found, in the online version, at doi:10.1016/j.cartre.2022.100226.

## References

[1] K. Kokubo, K. Matsubayashi, H. Tategaki, H. Takada, T. Oshima, Facile synthesis of highly water-soluble fullerenes more than half-covered by hydroxyl groups, ACS Nano 2 (2008) 327–333, doi:10.1021/nn700151z.
[2] K. Kokubo, S. Shirakawa, N. Kobayashi, H. Aoshima, T. Oshima, Facile and scalable synthesis of a highly hydroxylated water-soluble fullerenol as a single nanoparticle, Nano Res. 4 (2011) 204–215, doi:10.1007/s12274-010-0071-z.
[3] S. Afreen, K. Kokubo, K. Muthoosamy, S. Manickam, Hydration or hydroxylation: direct synthesis of fullerenol from pristine fullerene [C60] via acoustic cavitation in the presence of hydrogen peroxide, RSC Adv. 7 (2017) 31930–31939, doi:10.1039/C7RA03799F.
[4] S. Chokaouychai, Q. Zhang, Understanding phase-transfer catalytic synthesis of fullerenol and its interference from carbon dioxide and ozone, Res. Chem. Intermed. 46 (2020) 5391–5415, doi:10.1007/s11164-020-04269-7.
[5] L.O. Husebo, B. Sitharaman, K. Furukawa, T. Kato, L.J. Wilson, Fullerenols revisited as stable radical anions, J. Am. Chem. Soc. 126 (2004) 12055–12064, doi:10.1021/ja047593o.
[6] G.C. Alves, L.O. Ladeira, A. Righi, K. Krambrock, H.D. Calado, R.P. de F. Gil, M.V.B. Pinheiro, Synthesis of C60(OH)18-20 in aqueous alkaline solution under O2-atmosphere, J. Braz. Chem. Soc. 17 (2006) 1186–1190, doi:10.1590/S0103-50532006000600017.
[7] A. Djordjevic, B. Srdjenovic, M. Seke, D. Petrovic, R. Injac, J. Mrdjanovic, Review of synthesis and antioxidant potential of fullerenol nanoparticles, J. Nanomater. (2015) 1–15 2015, doi:10.1155/2015/567073.

[8] J. Zhuo, T. Wang, G. Zhang, L. Liu, L. Gan, M. Li, Salts of $C_{60}(OH)_8$ electrodeposited onto a glassy carbon electrode: surprising catalytic performance in the hydrogen evolution reaction, Angew. Chem. Int. Ed. 52 (2013) 10867–10870, doi:10.1002/anie.201305328.

[9] N.O. Mchedlov-Petrossyan, Fullerenes in liquid media: an unsettling intrusion into the solution chemistry, Chem. Rev. 113 (2013) 5149–5193, doi:10.1021/cr3005026.

[10] L.Y. Chiang, F.J. Lu, J.T. Lin, Free radical scavenging activity of water-soluble fullerenols, J. Chem. Soc. Chem. Commun. (1995) 1283, doi:10.1039/c39950001283.

[11] K. Kokubo, S. Yamakura, Y. Nakamura, H. Ueno, T. Oshima, Radical-scavenging Ability of Hydrophilic Carbon Nanoparticles: From Fullerene to Its Soot, Fuller. Nanotub. Carbon Nanostruct. 22 (2014) 250–261, doi:10.1080/1536383X.2013.812637.

[12] E. Castro, A.H. Garcia, G. Zavala, L. Echegoyen, Fullerenes in biology and medicine, J. Mater. Chem. B 5 (2017) 6523–6535, doi:10.1039/C7TB00855D.

[13] K. Kokubo, M.K. Espejo Cabello, N. Sato, Y. Uetake, H. Sakurai, Gold nanoparticles stabilized by molecular fullerenols, ChemNanoMat 6 (2020) 524–528, doi:10.1002/cnma.201900778.

[14] P. Chaudhuri, A. Paraskar, S. Soni, R.A. Mashelkar, S. Sengupta, Fullerenol−cytotoxic conjugates for cancer chemotherapy, ACS Nano 3 (2009) 2505–2514, doi:10.1021/nn900318y.

[15] T. Cao, Z. Wang, Y. Xia, B. Song, Y. Zhou, N. Chen, Y. Li, Facilitating electron transportation in perovskite solar cells via water-soluble fullerenol interlayers, ACS Appl. Mater. Interfaces 8 (2016) 18284–18291, doi:10.1021/acsami.6b04895.

[16] J.P.V. Damasceno, L.T. Kubota, Colloidal chemistry as a guide to design intended dispersions of carbon nanomaterials, Mater. Today Chem. 21 (2021) 100526, doi:10.1016/j.mtchem.2021.100526.

[17] J.P.V. Damasceno, F. Hof, O. Chauvet, A.J.G. Zarbin, A. Pénicaud, The role of functionalization on the colloidal stability of aqueous fullerene $C_{60}$ dispersions prepared with fullerides, Carbon 173 (2021) 1041–1047, doi:10.1016/j.carbon.2020.11.082.

[18] C. Mattevi, G. Eda, S. Agnoli, S. Miller, K.A. Mkhoyan, O. Celik, D. Mastrogiovanni, C. Cranozzi, E. Carfunkel, M. Chhowalla, Evolution of electrical, chemical, and structural properties of transparent and conducting chemically derived graphene thin films, Adv. Funct. Mater. 19 (2009) 2577–2583, doi:10.1002/adfm.200900166.

[19] G. Eda, C. Mattevi, H. Yamaguchi, H. Kim, M. Chhowalla, Insulator to semimetal transition in graphene oxide, J. Phys. Chem. C 113 (2009) 15768–15771, doi:10.1021/jp9051402.

[20] M.S. Dresselhaus, G. Dresselhaus, P.C. Eklund, Science of Fullerenes and Carbon Nanotubes, Elsevier, Orlando, Florida, USA, 1996.

[21] H. Mohan, D.K. Palit, J.P. Mittal, L.Y. Chiang, K.D. Asmus, D.M. Guldi, Excited states and electron transfer reactions of $C_{60}(OH)_{18}$ in aqueous solution, J. Chem. Soc. Faraday Trans. 94 (1998) 359–363, doi:10.1039/a705293f.

[22] A. Najafi, An investigation on dispersion and stability of water-soluble fullerenol ($C_{60}OH$) in water via UV–Visible spectroscopy, Chem. Phys. Lett. 669 (2017) 115–118, doi:10.1016/j.cplett.2016.12.030.

[23] F.F. Wang, N. Li, D. Tian, G.F. Xia, N. Xiao, Efficient synthesis of fullerenol in anion form for the preparation of electrodeposited films, ACS Nano 4 (2010) 5565–5572, doi:10.1021/nn100485g.

[24] D.J. Shaw, Introduction to Colloid and Surface Chemistry, 4th ed., Butterworth-Heinemann, Oxford, UK, 1992.

[25] R.J. Hunter, Foundations of Colloid Science, 2nd ed., Oxford University Press, New York, USA, 2001.

[26] G. Xing, J. Zhang, Y. Zhao, J. Tang, B. Zhang, X. Gao, H. Yuan, L. Qu, W. Cao, Z. Chai, K. Ibrahim, R. Su, Influences of structural properties on stability of fullerenols, J. Phys. Chem. B 108 (2004) 11473–11479, doi:10.1021/jp0487962.

[27] H.A. De Santiago, S.K. Gupta, Y. Mao, On high purity fullerenol obtained by combined dialysis and freeze-drying method with its morphostructural transition and photoluminescence, Sep. Purif. Technol. 210 (2019) 927–934, doi:10.1016/j.seppur.2018.08.033.

[28] A.L. Litvinov, D.V. Konarev, E.I. Yudanova, M.G. Kaplunov, R.N. Lyubovskaya, Selective reduction of fullerene $C_{60}$ by metals in neutral and alkaline media. Interaction of $C_{60}$ with KOH, Russ. Chem. Bull. 51 (2002) 2003–2007, doi:10.1023/A:1021695423077.

[29] A. Naim, P.B. Shevlin, Reversible addition of hydroxide to the fullerenes, Tetrahedron Lett. 33 (1992) 7097–7100, doi:10.1016/S0040-4039(00)60845-6.

[30] M. Wu, X. Wei, L. Qi, Z. Xu, A new method for facile and selective generation of $C_{60}^-$ and $C_{60}^{2-}$ in aqueous caustic/THF (or DMSO), Tetrahedron Lett. 37 (1996) 7409–7412, doi:10.1016/0040-4039(96)01613-9.

[31] X. Wei, M. Wu, L. Qi, Z. Xu, Selective solution-phase generation and oxidation reaction of $C_{60}^{n-}$ (n = 1,2) and formation of an aqueous colloidal solution of $C_{60}$, J. Chem. Soc. Perkin Trans. 2 (1997) 1389–1394, doi:10.1039/a607336k.

[32] C.A. Reed, R.D. Bolskar, Discrete fulleride anions and fullerenium cations, Chem. Rev. 100 (2000) 1075–1120, doi:10.1021/cr980017o.

[33] A. Hirsch, M. Brettreich, Fullerenes: Chemistry and Reactions, Wiley-VCH Verlag GmbH & Co. KGaA, Germany, 2005.

[34] M.S. Dresselhaus, G. Dresselhaus, A.M. Rao, P.C. Eklund, Optical properties of $C_{60}$ and related materials, Synth. Met. 78 (1996) 313–325, doi:10.1016/0379-6779(96)80155-X.

[35] K. Kokubo, Water-Soluble Single-Nano Carbon Particles: Fullerenol and Its Derivatives, InTech, 2012, doi:10.5772/36352.

[36] S. Deguchi, R.G. Alargova, K. Tsujii, Stable dispersions of fullerenes, $C_{60}$ and $C_{70}$, in water. Preparation and characterization, Langmuir 17 (2001) 6013–6017, doi:10.1021/la010651o.

[37] P.A. Indeglia, A. Georgieva, V.B. Krishna, J.C.J. Bonzongo, Physicochemical characterization of fullerenol and fullerenol synthesis by-products prepared in alkaline media, J. Nanopart. Res. 16 (2014), doi:10.1007/s11051-014-2599-4.

[38] H. Kuzmany, M. Matus, B. Burger, J. Winter, Raman Scattering in $C_{60}$ fullerenes and fullerides, Adv. Mater. 6 (1994) 731–745, doi:10.1002/adma.19940061004.

[39] S. Claramunt, A. Varea, D. López-Díaz, M.M. Velázquez, A. Cornet, A. Cirera, The importance of interbands on the interpretation of the raman spectrum of graphene oxide, J. Phys. Chem. C 119 (2015) 10123–10129, doi:10.1021/acs.jpcc.5b01590.

[40] A.C. Fingolo, J. Bettini, M. da Silva Cavalcante, M.P. Pereira, C.C.B. Bufon, M. Santhiago, M. Strauss, Boosting electrical conductivity of sugarcane cellulose and lignin biocarbons through annealing under isopropanol vapor, ACS Sustain. Chem. Eng. 8 (2020) 7002–7010, doi:10.1021/acssuschemeng.0c00320.

[41] E. Ravelo-Nieto, A. Duarte-Ruiz, L.H. Reyes, J.C. Cruz, Synthesis and characterization of a fullerenol derivative for potential biological applications, Mater. Proc. 4 (2021) 15, doi:10.3390/IOCN2020-07793.

[42] P.R. Birkett, H.W. Kroto, R. Taylor, D.R.M. Walton, R.Ian Grose, P.J. Hendra, P.W. Fowler, The Raman spectra of $C_{60}Br_6$, $C_{60}Br_8$ and $C_{60}Br_{24}$, Chem. Phys. Lett. 205 (1993) 399–404, doi:10.1016/0009-2614(93)87141-O.

[43] X. Li, F. Kang, M. Inagaki, Buckybowls: corannulene and its derivatives, Small 12 (2016) 3206–3223, doi:10.1002/smll.201503950.

[44] W. Krätschmer, L.D. Lamb, K. Fostiropoulos, D.R. Huffman, Solid $C_{60}$: a new form of carbon, Nature 347 (1990) 354–358, doi:10.1038/347354a0.

[45] B. Vileno, P.R. Marcoux, M. Lekka, A. Sienkiewicz, T. Fehér, L. Forró, Spectroscopic and photophysical properties of a highly derivatized $C_{60}$ fullerol, Adv. Funct. Mater. 16 (2006) 120–128, doi:10.1002/adfm.200500425.

[46] J.D. Saxby, S.P. Chatfield, A.J. Palmisano, A.M. Vassallo, M.A. Wilson, L.S.K. Pang, Thermogravimetric analysis of buckminsterfullerene and related materials in air, J. Phys. Chem. 96 (1992) 17–18, doi:10.1021/j100180a007.

[47] S. Aghili, M. Panjepour, M. Ghiaci, Degradation mechanism and oxidation kinetics of $C_{60}$ fullerene, Diam. Relat. Mater. 124 (2022) 108943, doi:10.1016/j.diamond.2022.108943.

[48] S. Lunell, C. Enkvist, M. Agback, S. Svensson, P.A. Brühwiler, Core photoionization satellites in fullerene and related model systems, Int. J. Quantum Chem. 52 (1994) 135–146, doi:10.1002/qua.560520114.

[49] Y.M. Shulga, V.M. Martynenko, V.V. Open'ko, A.V. Kulikov, A. Michtchenko, E. Johnson, M.D. Mochena, G.L. Gutsev, Oxidation of $C_{60}$ fullerite by interstitial oxygen, J. Phys. Chem. C 112 (2008) 12096–12103, doi:10.1021/jp710745f.

[50] P. Zygouri, K. Spyrou, E. Mitsari, M. Barrio, R. Macovez, M. Patila, H. Stamatis, I.I. Verginadis, A.P. Velalopoulou, A.M. Evangelou, Z. Sideratou, D. Gournis, P. Rudolf, A facile approach to hydrophilic oxidized fullerenes and their derivatives as cytotoxic agents and supports for nanobiocatalytic systems, Sci. Rep. 10 (2020) 1–13, doi:10.1038/s41598-020-65117-7.

[51] D. Friedrich, K. Henkel, M. Richter, D. Schmeißer, Fullerenol as probed by synchrotron X-ray photoemission and absorption spectroscopy, Bionanoscience 1 (2011) 218–223, doi:10.1007/s12668-011-0025-2.

[52] F. Hof, S. Bosch, S. Eigler, F. Hauke, A. Hirsch, New basic insight into reductive functionalization sequences of single walled carbon nanotubes (SWCNTs), J. Am. Chem. Soc. 135 (2013) 18385–18395, doi:10.1021/ja4063713.